Synthesis of gold nanorods with small thiolated molecules

Katherinne I. Requejo Roque[1], Anton V. Liopo[1,2], and Eugene R. Zubarev[1]
[1]Department of Chemistry, Rice University, [2]Institute for Bioscience and Technology, Texas A&M University

Introduction

Towards the high yield synthesis of small gold nanorods by using bioadditives during growth

Gold nanorods (AuNRs) are one of the most studied anisotropic nanoparticles because of their unique optical properties [1]. Besides, AuNRs have attracted great attention because their distinct sizes can enable applications in sensing, biomedical imaging and photothermal therapy [2, 3].

AuNRs are characterized by the surface plasmon resonance (SPR) which is a collective oscillation of the conduction band electrons of gold upon interaction with light of certain frequency. The plasmon absorption of AuNRs (**Figure 1**) splits into two bands: the transverse and longitudinal surface plasmon resonances (TSPR and LSPR) in which the position of the latter band depends on the nanorods aspect ratio (AR).

Despite many reports on the broad LSPR band tunability and improvement of shape yield for the seed-mediated method [4, 5], there are few studies on the seedless synthesis of small AuNRs in high yield, their reproducibility and scalability.

Here, we describe novel seeded and seedless protocols of AuNRs by using small thiolated molecules such as glutathione (GSH), oxidized glutathione (GSSG), L-cysteine (L-cys) and L-methionine (L-met) during growth. Our reproducible and scalable protocol produces AuNRs of different dimensions and aspect ratios depending on the concentration and addition time of the bioadditive. Interestingly, the nanorod growth is accelerated in the presence of the bioadditives but only glutathione enables the high yield synthesis of small AuNRs [6].

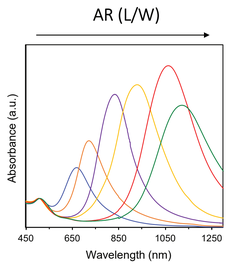

Figure 1. Variation of optical properties of AuNRs by changing the aspect ratio (AR, length/width).

Experimental Strategy

Nanomolar concentrations of bioadditives during AuNRs growth

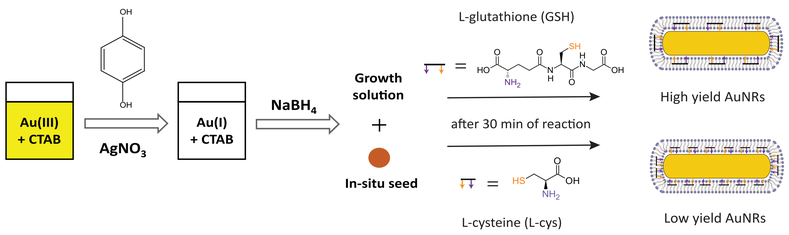

Figure 2. Scheme of AuNRs seedless synthesis with hydroquinone as weak reducing agent. The surfactant is cetyltrimethylammonium bromide (CTAB).

Surface characterization and AuNRs functionalization with PEG-SH and MUTAB

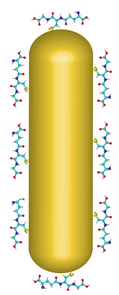

Figure 3. Representation of some GSH molecules adsorbed on AuNR surface.

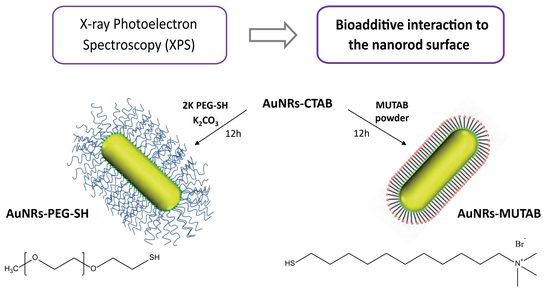

Figure 4. CTAB is replaced from AuNRs surface with thiolated polyethylene glycol (PEG-SH) and 11-mercaptoundecyltrimethylammonium bromide (MUTAB) in aqueous solution.

Results

Effect of concentration and addition time of GSH: small amounts of GSH blue-shift the LSPR band and AuNRs quality improves in the seedless protocol

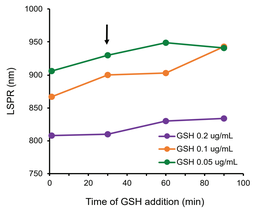

Figure 5. Variation of LSPR band based on GSH addition time and concentration for the seedless method of AuNRs.

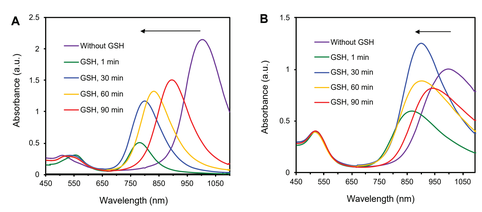

Figure 6. Time-dependent normalized UV-Vis spectra of AuNRs synthesized with GSH by the (A) seeded and (B) seedless methods in 100 mM CTAB. GSH at 0.1 μg/mL added during the first 90 min of growth.

Reduction in AuNRs aspect ratio with nanomolar concentrations of GSH

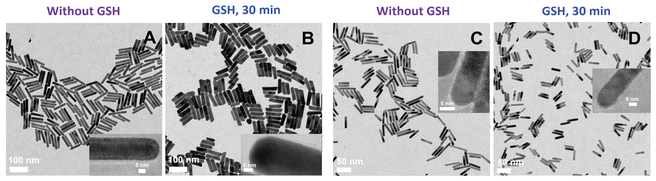

Figure 7. TEM and HR-TEM (inset) images of AuNRs after overnight growth for the (A-B) seeded and (C-D) seedless syntheses. AuNRs (A, C) without GSH and (B, D) with 0.1 μg/mL GSH added at 30 min after initiation of growth. Scale bars indicate 100, 50 and 5 nm.

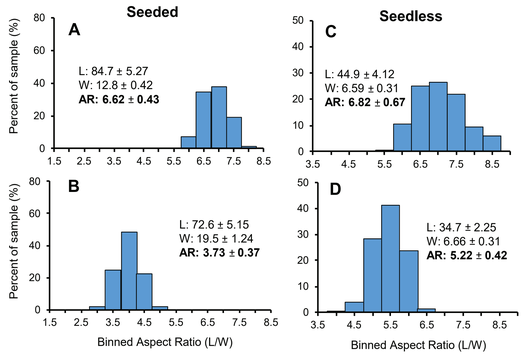

Figure 8. Histograms of AuNRs aspect ratio distributions for the (A-B) seeded and (C-D) seedless syntheses. AuNRs (A, C) without GSH and (B, D) with 0.1 μg/mL GSH added at 30 min after growth. Length (L) and width (W) are in nm.

The shape yield is enhanced by using GSH in the seedless protocol. Regardless of the GSH concentration, the AuNRs morphology is not affected. Reshaping of nanorods tip is observed in the seeded method (**Figure 7**).

As the concentration of GSH increases, the aspect ratio of AuNRs decreases due to a reduction in length for both protocols (**Figure 8**).

High yield synthesis of AuNRs with GSSG and L-met but low quality with L-cys

Table 1. LSPR band position, shape yield and dimensions for AuNRs synthesized by the seeded and seedless methods without and with bioadditives.

Sample	[Bioadditive] μg/mL	LSPR or λmax* (nm)	% Shape yield	Length/Width (nm)	AR
Control	-	1015	96	L: 84.7 ± 5.27 W: 12.8 ± 0.42	6.62 ± 0.43
GSSG	0.2	998	95	L: 100.6 ± 4.42 W: 18.2 ± 0.54	5.52 ± 0.28
L-cys	0.2	574*	<30	L: 37.3 ± 4.08 W: 18.2 ± 1.98	2.06 ± 0.27
L-met	0.2	1032	98	L: 89.2 ± 4.05 W: 13.4 ± 0.36	6.66 ± 0.33
Control	-	1000	86	L: 44.9 ± 4.12 W: 6.59 ± 0.31	6.82 ± 0.67
GSSG	0.1	946	92	L: 36.8 ± 3.88 W: 6.12 ± 0.23	6.00 ± 0.71
L-cys	0.2	710	40	L: 14.7 ± 1.60 W: 6.41 ± 0.30	2.30 ± 0.28
L-met	0.025	1047	87	L: 49.7 ± 4.35 W: 6.69 ± 0.22	7.42 ± 0.73

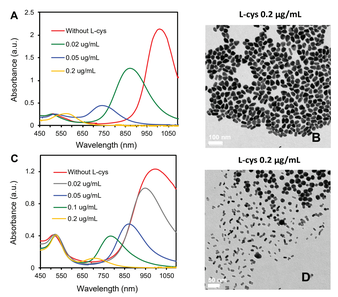

Figure 9. Normalized UV-Vis spectra and TEM images of AuNRs synthesized with L-cys added at 30 min of growth for the (A, B) seeded and (C, D) seedless methods.

Results

Kinetics of nanorod growth for glutathione and L-cysteine

AuNRs grown with small amounts of GSH and L-cys tend to have lower LSPR wavelengths with more rapid growth. In the presence of the bioadditives, the nanorod growth is accelerated by more than two times as compared to the control (**Figure 10A**).

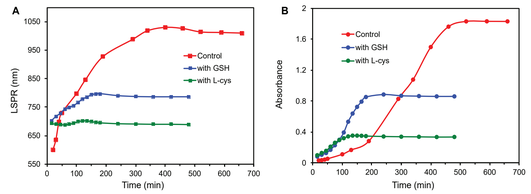

Figure 10. Variation of AuNRs LSPR band position (A) and its absorbance (B) as a function of time for the seedless method. AuNRs control (red), with 0.2 μg/mL GSH (blue) and L-cys (green) added at 30 min after $NaBH_4$.

The fast nanorod formation with GSH and L-cys produces saturation of the absorbance at earlier reaction time (**Figure 10B**). Thus, when small thiolated compounds are incorporated during growth, the stabilization of the growing nanorods occurs in a shorter period of time.

XPS confirmation of Au-S interaction between AuNRs and bioadditives

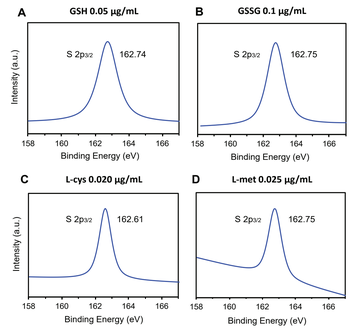

Figure 11. High resolution XPS spectra of S 2p for AuNRs with (A) 0.05 μg/mL GSH, (B) 0.1 μg/mL GSSG, (C) 0.02 μg/mL L-cys and (D) 0.025 μg/mL L-met added at 30 min after $NaBH_4$ (seedless synthesis).

Enhanced colloidal stability with GSH and L-cys for MUTAB coated AuNRs

Table 2. Zeta potential (mV) of AuNRs before and after surface modification with 2K PEG-SH and MUTAB. AuNRs control and with bioadditives at the same molar concentration of 165 nM (seedless method).

Sample	Control	GSH	GSSG	L-cys
CTAB	44.5 ± 3.0	49.9 ± 1.2	41.1 ± 1.2	40.4 ± 2.5
PEG-SH	-27.1 ± 1.3	-37.8 ± 0.5	-31.7 ± 1.0	-31.4 ± 0.4
MUTAB	44.4 ± 6.0	**61.7 ± 2.2**	42.6 ± 0.9	**55.8 ± 3.0**

The absence of the less intense S $2p_{1/2}$ peak at higher binding energy is because of the low concentration of bioadditives adsorbed on AuNRs (**Figure 11**).

The distinct effects of these small thiolated molecules are attributed to their adsorption strength (thiol, disulfide and thioether).

Conclusions

- Small amounts of bioadditives added during growth produce AuNRs with tunable LSPR band depending on the bioadditive concentration and addition time.
- In this novel seedless synthesis, the nanorod growth is accelerated by more than two times in the presence of GSH and L-cysteine.
- Our reproducible and scalable seedless protocol enables the synthesis of AuNRs with smaller sizes and the nanorod morphology is preserved.
- Only GSH and GSSG produce AuNRs in high yield and the colloidal stability of nanorods containing glutathione is enhanced after functionalization with MUTAB.
- Future studies may explore the incorporation of other additives in nanomolar concentrations to improve the quality of other anisotropic shapes for diverse applications.

Acknowledgements

We gratefully acknowledge the financial support provided by the National Science Foundation (DMR-1105878). Thanks to Dr. Zubarev and Dr. Liopo for their support on the project and for their suggestions on how to guide the present investigation.
Contact information: kirequejo@gmail.com

REFERENCES:
[1] Vigderman, L. et al. *Adv. Mater.* **2012**, *24*, 4811-4841.
[2] Pérez-Juste, J. et al. *Coordin. Chem. Rev.* **2005**, *249*, 1870-1901.
[3] Li, Z. et al. *ACS Biomater. Sci. Eng.* **2016**, *2*, 789-797.
[4] Murphy, C. J. et al. *Curr. Opin. Colloid. In.* **2011**, *16*, 128-134.
[5] Ye, X. et al. *Nano Lett.* **2013**, *13*, 765-771.
[6] Requejo, K. I. et al. *Langmuir* **2020**, *36*, 3758-3769.

Selective Attachment of Covalent Organic Frameworks to 2D Nanomaterials

Lucas K. Beagle[1,2], Ly D. Tran[1,2], Luke A. Baldwin[1], Nicholas R. Glavin[1]

[1] AFRL, Wright-Patterson AFB, OH, United States.
[2] UES, Inc., Beavercreek, OH, United States.

LEAD | DISCOVER | DEVELOP | DELIVER

Abstract

Chemical sensing using 2-D nanomaterials has been an area of intense investigation exhibiting high sensitivity, however it has been limited as a field due to the lack of selectivity among analytes. Covalent organic frameworks are large porous and repeated organic frameworks which have been shown to act as selectivity agents due to functionalization and porosity. This research focuses on the association of COFs with 2-D nanomaterials using bottom-up and top-down design methodologies and investigated under solvothermal and microwave assisted synthesis. Several known COF species have been examined in order to understand the fundamental surface interactions between 2-D nanomaterials and COFs.

Chemical Sensing

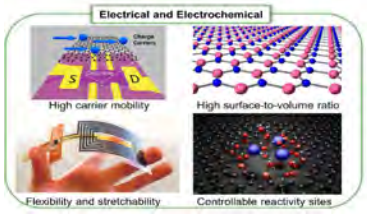

Chemical Sensing is a relevant and challenging field. While changes in optical and electrical measurements are used to determine values in concentration, selectivity is not inherent and therefore an essential area of investigation.

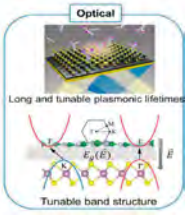

2-D Nanomaterials

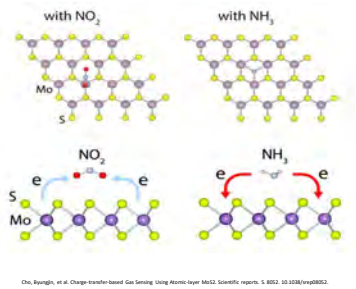

- Typical sensing with TMDs occurs via monitoring changes in electrical properties in response to surface adsorption of analytes
  - Analyte will either be an electron donor (NH_3) or an electron acceptor (NO_2)
- Depending on the type of dopant and nature of the material (p type or n type), an increase or decrease in resistance will occur:
  - For p-type materials:
    - Electron Donors → Resistance ↑
    - Electron Acceptors → Resistance ↓
  - For n-type materials:
    - Electron Donors → Resistance ↓
    - Electron Acceptors → Resistance ↑

Covalent Organic Frameworks (COF)

Reticular Networks of organic linker and vertices. The highly repeatable network allows for the design and modification of pores to fit or interact with desired analytes.

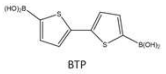

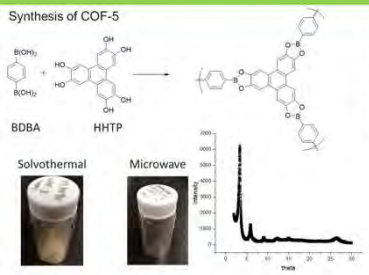

Building of the network occurs through monomer cross-condensation into moieties such as boronate esters and imine functional groups.

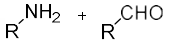

Sensors with 2D organic and inorganic materials

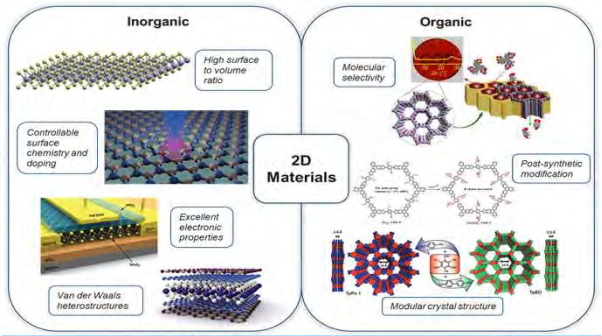

Marriage of the sensitivity of the inorganic 2-D TMD surface with the selectivity of the organic COF surface. Differing material combinations will be employed in order to maximize performance

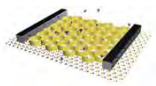

Devices

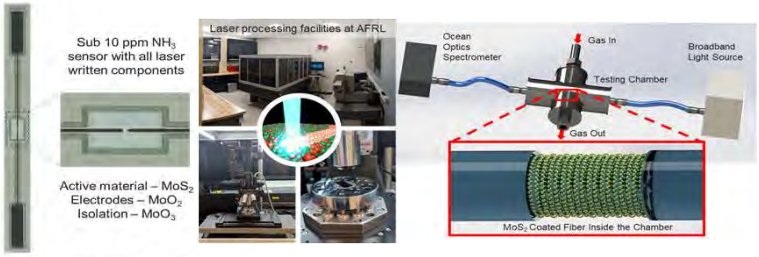

Devices are manufactured in-house, leveraging our expertise in materials synthesis. Resistance based measurements are carried out using custom made transducers. Our novel conversion of amorphous MoS_2 via laser-induced crystallization into 2H-MoS_2 and further transformation into MoO_2 and MoO_3. Refractive index changes are exhibited in our materials in our proprietary optical sensing devices.

COF Thin Films

Top-down synthesis of thin films of COF-5 were attempted under both solvothermal and microwave conditions, Microwave conditions produced interesting results where selective nucleation occurs on MoCVD grown $MoSe_2$ crystals, leading to a microwave induced effect due to selective excitation of the TMD crystals.

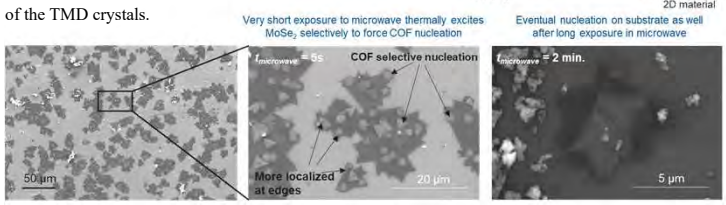

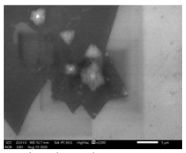

Imine-based COF nucleation on $MoSe_2$ flakes

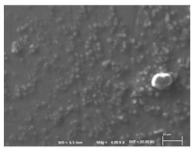

Imine-based COF over large area of MoS_2 on Silicon wafers.

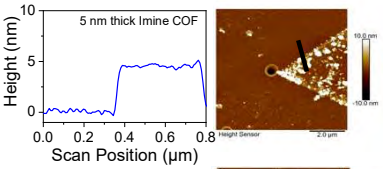

Image correlation to study growth kinetics.

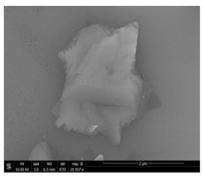

Boronate ester-based COF deposition on $MoSe_2$.

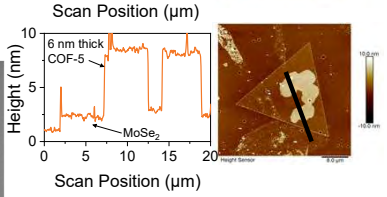

AFM images showing the height of flakes attached to $MoSe_2$ flakes. (Top imine-based, bottom COF-5)

Conclusions

We have demonstrated the ability to selectively attach imine-based and boronate ester COF selectively to TMD surfaces. These advances open the doors to future work in synthesis and development of novel Organic-Inorganic based 2D sensors.

Special thanks to the Lou Group at Rice University for the MoCVD grown flakes, Mr. David Moore for AFM images

Functionalization of Nanoparticles with Temperature and pH activated Smart Polymers for Controllable Self-Assembling Systems

Buddhini C. N. Vithanage*, Mathew M. Maye

*bcnugadu@syr.edu, *mmmaye@syr.edu*

Department of Chemistry, Syracuse University
Syracuse, New York

❖ Background

Smart polymers are high-performance polymers that can alter according to the environment they are in and they can be respond to temperature, pH, light or other external stimuli. The surface modification of gold nanoparticles (AuNPs) with smart polymers has a diverse range of applications in self-assembly, drug delivery, and sensing.

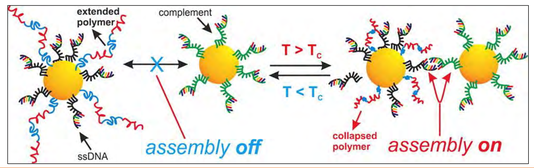

ACS Nano **2013**, *7*, 7011
Langmuir **2013**, *29*, 15217

❖ Smart Polymer Synthesis and Characterization

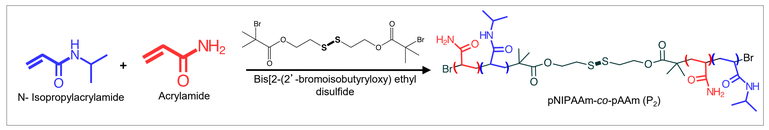

Thermosensitive Co-polymer Synthesis: Low critical solution temperature (LCST) thermosensitive co-polymers (pNIPAAm-co-pAAm) were synthesized using a disulfide initiator. Initiator allows for attachment to the gold nanoparticles (AuNPs) surface. By changing the ratio between two monomers, co-polymers with different LCST were successfully synthesized.

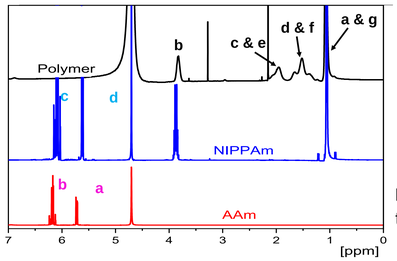

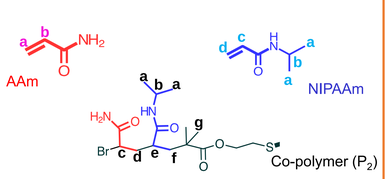

NMR: ^{1}H-NMR measurements were used to confirm the co-polymer structures.

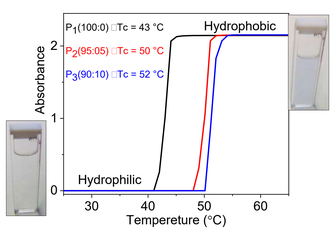

LCST Determination: Using thermal UV-Vis measurements, the transition temperature (T_C) of synthesized co-polymers was determined.

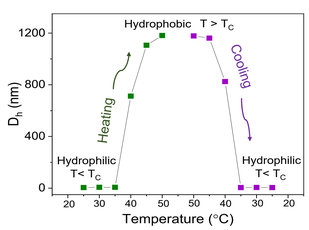

DLS measurements: DLS data of co-polymer (P_2) showed the reversible temperature induced conformational change of the synthesized co-polymers.

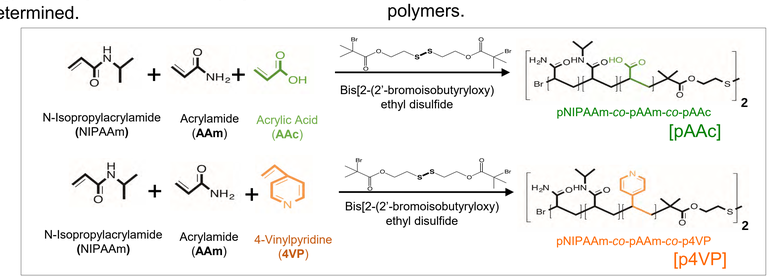

pH-sensitive Co-polymer Synthesis: Stimuli responsive co-polymers (pNIPAAm-*co*-pAAm-*co*-pAAc and pNIPAAm-*co*-pAAm-*co*-p4VP) having a disulfide linkage were successfully synthesized through an Atom Transfer Radical Polymerization.

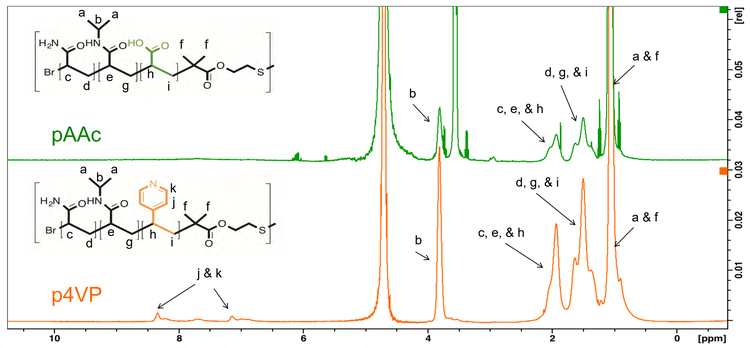

NMR: ^{1}H-NMR confirmed AAc and 4VP functionality in synthesized pH sensitive co-polymer structures.

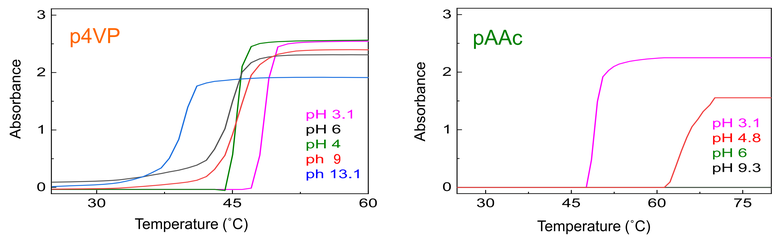

LCST Determination: Using thermal UV-Vis measurements the LCST's were determined, and found sensitive to pH. Changing pH disrupts charge, which in turn alters H-bonding, leading to varied LCST transitions.

❖ Co-polymer Capped 'Smart AuNPs'

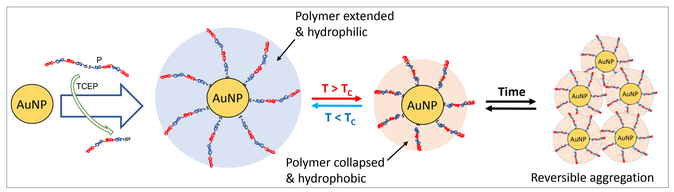

The co-polymers were attached to the AuNPs by reducing the disulfide linkage using TCEP. The reduced co-polymer in thiol form is then added to the AuNPs and incubated overnight. After purification, thermosensitive and pH-sensitive assemble is accomplished by changing the temperature above and below the polymer T_C. When $T < T_C$, polymer is hydrophilic. When $T > T_C$, polymer is hydrophobic and with the time AuNPs reversibly assemble.

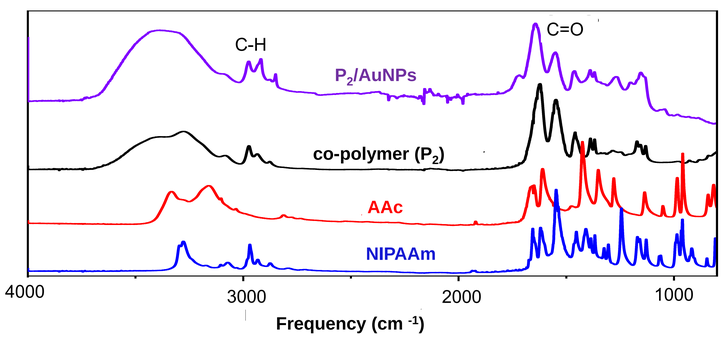

FTIR : FTIR confirmed the polymer composition, and NP functionalization. Co-polymer spectrum showed individual monomer stretching peaks including, $-CH_2$ and $-CH_3$ stretching around ~2900 cm^{-1} , and primary and secondary amide stretches around ~1700 cm^{-1}.

❖ Temperature and pH Study of 'Smart AuNPs'

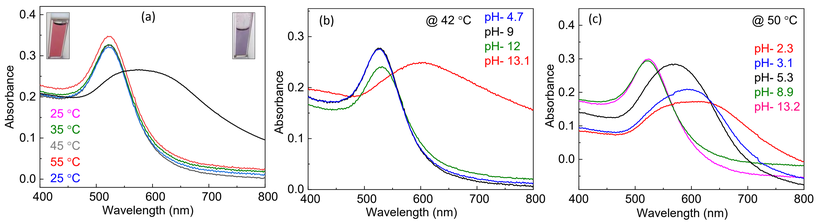

Broadening of the AuNPs surface plasmon resonance band (SPR) is an indication of close inter-particle distances ($d < D_{Au}$). The nanoparticle SPR broadening corresponded with T>Tc (a), or change in pH (b & c). Notice the opposite aggregation behaviour of the p4VP and pAAc functionalized particles in b and c, respectively.

❖ Zeta Potential Study of Co-polymers and 'Smart AuNPs'

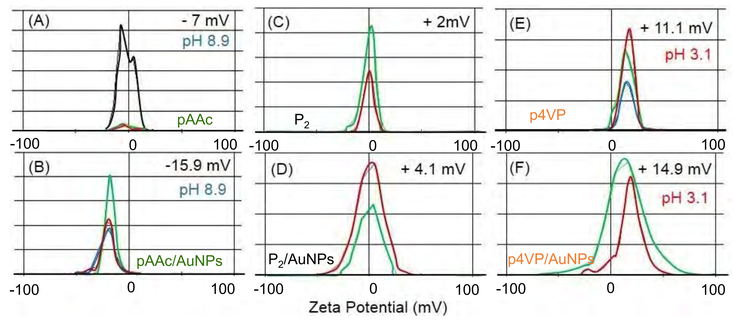

Zeta Potential: Under basic to acidic conditions (3.1< pH <8.9) thermosensitive co-polymer (P_2) was shown zeta potential of +2 mV and P_2/AuNPs system was shown zeta potential of + 4.1 mV. Under identical conditions pAAc had a zeta potential of -7.0 mV and p4VP had a zeta potential of +11.1mV. Also pAAc/AuNPs had a zeta potential of -15.9 mV and p4VP/AuNPs had a zeta potential of +14.9 mV.

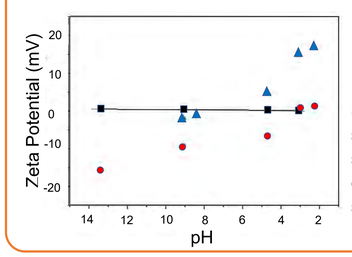

- p4VP/ AuNPs
- pAAc/ AuNPs
- P_2/ AuNPs

Systematic study on how overall charge of co-polymer/AuNPs system change with the solution pH (2.1< pH > 13.4). Study shows that changing overall pH can change the charge of the co-polymer/AuNPs systems to neutral, depending on their specific pKa profiles.

❖ Summary

The resulting thermo-responsive co-polymers have a transition temperatures (T_C) varying from 43 ˚C to 52 ˚C. The thermos-responsive behaviour of the co-polymers allowed for the reversible self-assembly of the nanoparticles once they were grafted on to the AuNPs. The resulting pH sensitive co-polymers are sensitive to changes in both temperature and pH. The zeta potential analysis shows co-polymer with AAc is negatively charged and co-polymer with 4VP is positively charged with the magnitude of the charges dependent on each polymers pKa profile. Based on zeta potential study, charge and the magnitudes of charge of co-polymer functionalized systems can be tuned by changing solution pH. This open new way for studying the electrostatic assembly of nanoparticles in charged systems.

❖ References

1. Hamner, K. L.; Alexander, C. M.; Coopersmith, K.; Reishofer, D.; Provenza, C.; Maye, M. M. *Acs Nano* **2013**, *7*, 7011-7020.
2. Hamner, K. L.; Maye, M. M. *Langmuir* **2013**, *29*, 15217-15223.
3. Yavuz, M. S.; Cheng, Y.; Chen, J.; Cobley, C. M.; Zhang, Q.; Rycenga, M.; Xie, J.; Kim, C.; Song, K. H.; Schwartz, A. G. *Nature materials* **2009**, *8*, 935.

Examining the role of chloride surface ligands on dislocation removal dynamics in imperfectly attached CdSe/CdS nanocrystals

Amy McKeown-Green[†], Justin Ondry[†‖], A. Paul Alivisatos[†‖⊥‡]

[†]Department of Chemistry, University of California, Berkeley, California 94720, United States, [‖]Kavli Energy NanoScience Institute, Berkeley, California 94720, United States, [‡]Materials Sciences Division, Lawrence Berkeley National Laboratory, Berkeley, California 94720, United States, [⊥]Department of Materials Science and Engineering, University of California, Berkeley, California 94720, United States

Oriented attachment of CdSe/CdS nanoparticles

Oriented attachment is a useful crystal growth process in synthetic nanomaterials. However, it is limited by its irreversibility which causes defects at the attachment interface between two nanoparticles, such as dislocations, to be locked into place. To address this limitation, we sought to develop methods for facilitating dislocation removal in imperfectly attached nanoparticles. The introduction of chloride ligands to CdX (X=S, Se, Te) semiconductor nanoparticles has been shown to increase grain growth in nanocrystal thin films as well as lower the zinc blend-wurtzite phase transition temperature upon annealing. In this work, dislocation removal in imperfectly attached CdSe/CdS core-shell nanocrystals with and without chloride surface ligands was studied using *in-situ* high-resolution transmission electron microscopy.

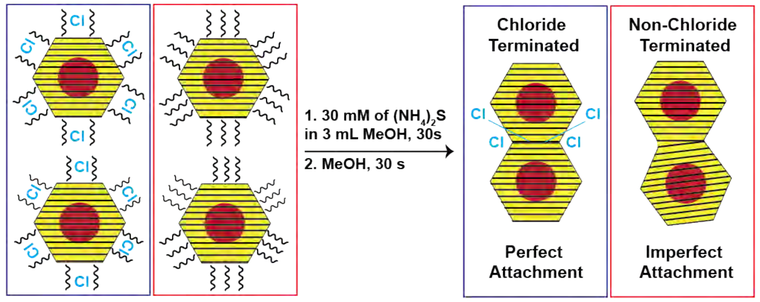

Introduction of Chloride Surface Ligands

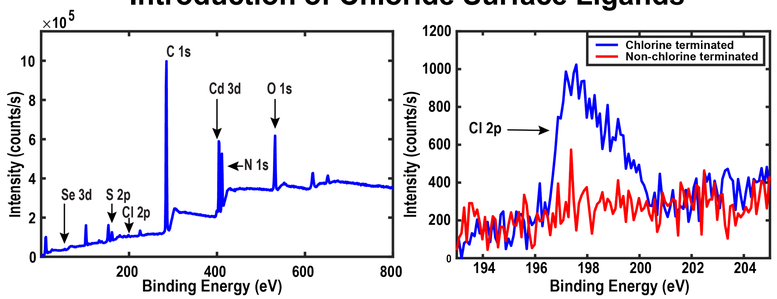

Chloride surface ligands were introduced to an aliquot of the parent nanoparticle solution via heating to <270°C for 1 hour in the presence of Cetyltrimethyl ammonium chloride (CTAC).

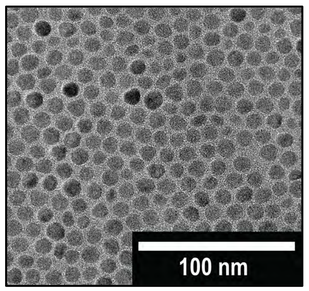

X-ray photoelectron spectroscopy (XPS) confirmed the presence of chlorine in the treated sample. No chlorine was observed in the untreated sample.

Post-CTAC treatment, the particles were observed to maintain their hexagonal prism shape and wurtzite crystal structure.

Dislocation Removal Trajectories in Both Non-Chloride Terminated and Chloride Terminated Nanoparticles

Non chloride-terminated CdSe/CdS core shell nanoparticles

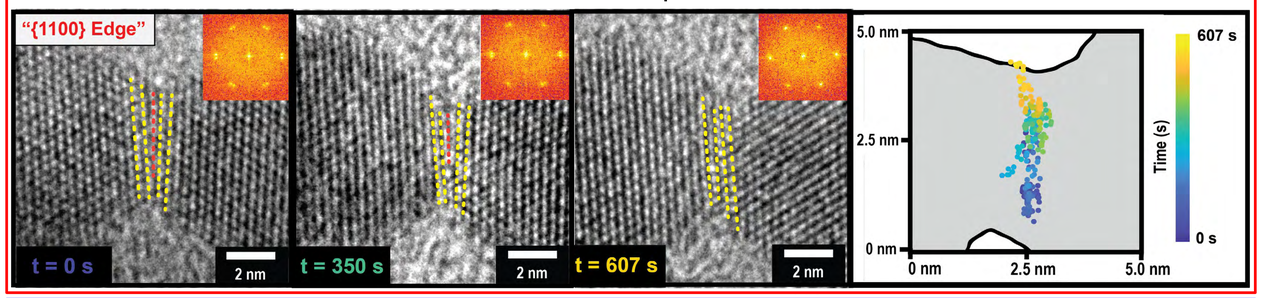

Chloride-terminated CdSe/CdS core shell nanoparticles

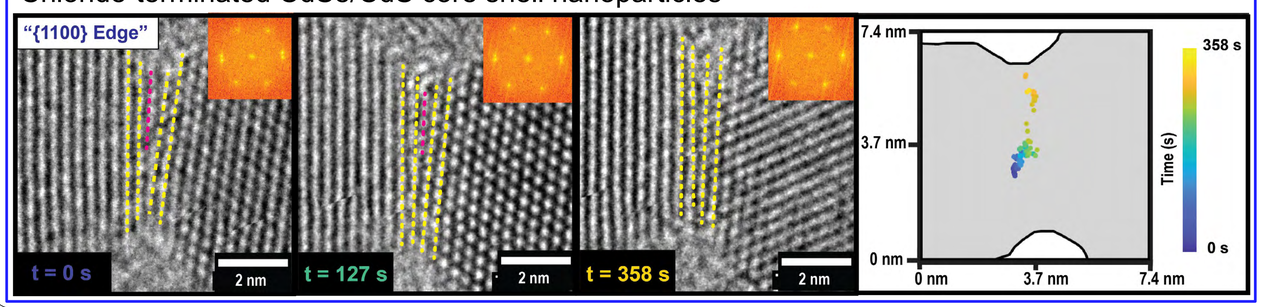

The wurtzite CdSe/CdS nanocrystals used had a hexagonal prism shape and were terminated predominantly with {1100} facets. Following treatment with $(NH_4)_2S$, orientated attachment was observed primarily on {1100} facets. In the case of imperfect attachment, b=$\frac{a}{3}$<$2\bar{1}\bar{1}0$> edge dislocations were observed.

In both cases, the observed mechanism of removal was dislocation climb, with the edge dislocation moving out of its slip plane to traverse the shortest distance to the surface.

Dislocation Removal times in Non-chloride terminated and chloride terminated nanoparticles

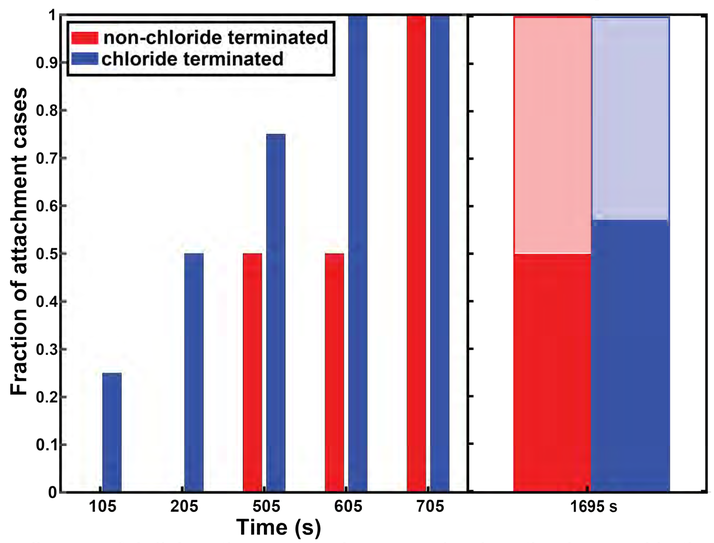

Successful dislocation removal was predominantly observed in the chloride-terminated sample. When full dislocation removal was observed in both chloride terminated and non-chloride terminated attachment cases, the chloride terminated samples showed faster removal times.

Future Work: Chloride treatment post-SILAR

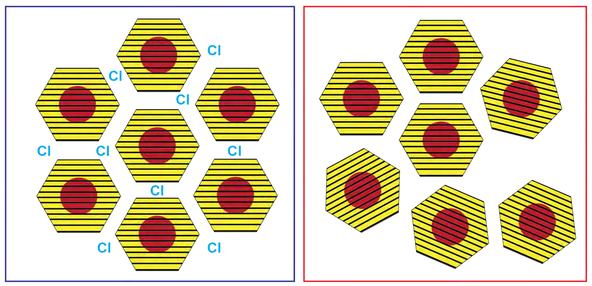

We are interested to observe whether treating assembled arrays on CdSe/CdS nanoparticles with CTAC or another chloride-based ligand results in better attachment interfaces across the array as a whole, resulting in larger grain sizes with lower angle tilt boundaries.

Acknowledgements

This work was supported by the National Science Foundation, Division of Materials Research (DMR), under Award Number DMR-1808151. Portions of this work were performed at the Molecular Foundry supported by the Office of Science, Office of Basic Energy Sciences, of the U.S. Department of Energy under Contract No. DE-AC02-05CH11231. J.C.O acknowledges the support of the Kavli Philomathia Graduate Student Fellowship.

Contact information: amy_mckeown-green@berkeley.edu

Stabilities of adsorption structures of 2,4,6-tris(4-bromophenyl)-1,3,5-triazine on Au(111) surface

Arifumi Okada[1*], Shingo Hasui[2], Shinsuke Hara[3], Kosuke Mino[2], Masamichi Yoshimura[4], and Kohei Kadono[1]

[1]Faculty of Materials Science and Engineering, Kyoto Institute of Technology
[2]Graduate School of Science and Technology, Kyoto Institute of Technology
[3]National Institute of Information and Communications Technology
[4]Toyota Technological Institute
*Email: aokada@kit.ac.jp

Introduction

Monolayers of 2,4,6-tris-(4-Bromophenyl)-1,3,5-triazine (TBPT) on Au(111) surfaces show several molecular arrangements, partially similar to the case of 1,3,5-tris(4-bromophenyl)benzene (TBPB) [1]. In the TBPT molecular array fabrication through solvent evaporation, a phase different from that observed at the solid-liquid interface [2] was found. This phase, in which Br-N interaction is apparently dominant, has low reactivity to dimerize [3]. In order to obtain well-extended covalent bonded molecular network, it is important to understand the origin of structural stabilities of molecular arrangement phases. In the present study, we focus on this low-reactivity phase and investigate molecule-substrate and intermolecular interactions using density functional theory (DFT) calculations.

Experimental method

Sample preparation: solvent evaporation

Au was deposited on mica and annealed → Solution applied (0.05 mM in 1,4-butanediol) → Solvent evaporated on a hot plate (70 ~ 150 °C)

T / °C	Evaporation time / min
70	220
80	135
100	75
150	5

Surface observation: scanning tunneling microscopy (STM)

In air, using PtIr (80/20) wire as a tip
Constant current mode (sample bias voltage: +0.1 V, tunneling current: 0.2 nA)

Experimental results [3]

Solvent evaporation at 80°C (135 min)

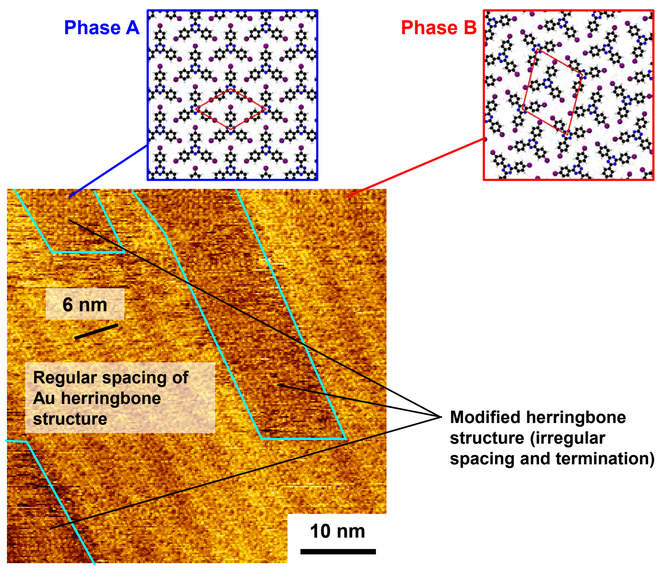

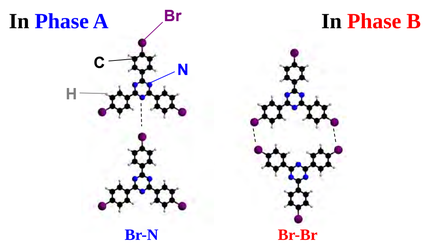

After 80°C evaporation, two molecular arrangements were observed.

Arrangement through Br-N interaction: 'Phase A' → formed at lower evaporation temperature (rate)

Arrangement through Br-Br interaction: 'Phase B'

Phase A: dominant after 70°C evaporation (lower temperature)
Phase B: dominant after 90°C evaporation
→ Other phase was observed after 100°C evaporation, and dimerization was observed after 150°C evaporation

- Au herringbone structure was lifted up at phase A
- After additional annealing of phase B in air (~ 150°C), phase A was dominantly observed.
→ Once phase A formed, dimerization does not occur.

- Formation of the phase A: feasible at slow evaporation
- Molecule-substrate interaction of phase A is stronger than that of phase B

→ Phase A is more stable than phase B, but kinetically unfavorable

Solvent evaporation at 150°C (5 min)

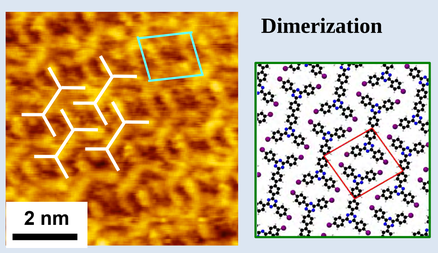

Dimerization occurs at higher evaporation temperature (higher evaporation rate).

Model construction for DFT calculations

First we focus on phase A.
In the present study both gas-phase (pairwise) and adsorption were investigated.

Single molecule and molecular pair

Package: GAMESS [4]
Functional: B3LYP for single molecule
B3LYP-D3 for molecular pair
Basis set: 6-311G** for single molecule
6-31G** for molecular pair
Symmetry: C_3 for single molecule
D_{2h} or D_{2v} for molecular pair

TBPT/Au (periodic boundary condition)

Package: Quantum ESPRESSO [5,6]
Functional: rev-vdW-DF2 [7]
Pseudopotential: PBE-USPP [8]

Pairwise interaction in gas phase (GAMESS)

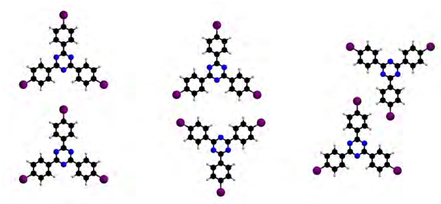

Phase A	Phase B_a	Phase B_b
– 0.139 eV	– 0.201 eV	– 0.140 eV

→ Similar magnitude to the case of other molecules [9].

Br-N interaction: weaker than Br-Br.

Adsorption model (Quantum ESPRESSO)

Lateral unit cell sizes are based on calculated lattice constant of bulk Au

Unit cell (non-rotated, see below)

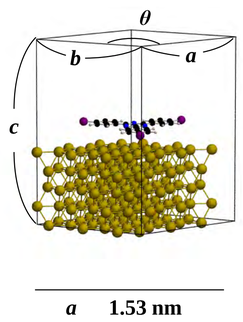

a	1.53 nm
b	1.53 nm
c	2.50 nm
θ	120°

Unit cell (isolated molecule)

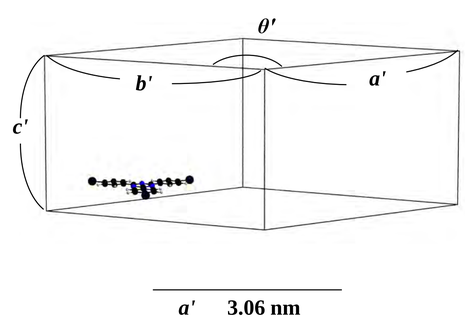

a'	3.06 nm
b'	3.06 nm
c'	2.00 nm
θ'	120°

Adsorption site: defined by center of molecule

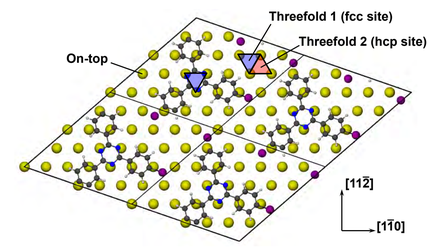

(Molecule: 'rotated' configuration)

In this study, two types of molecular orientations were considered.
(1) Unit cell with mirror symmetry: 'non-rotated'
(2) TBPT was rotated by 10.9° so that the molecular center and Br atoms occupy the same kind of site: 'rotated'

Examples of molecular arrangements

Molecular center: on-top site

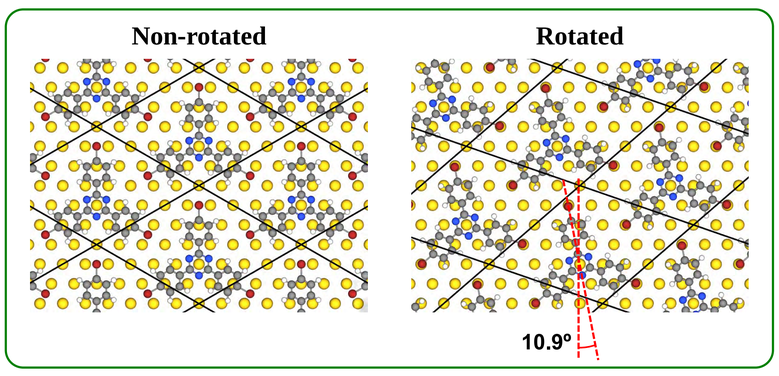

Occupied sites

Non-Rotated

	Threefold 1	Threefold 2	On-top
center	fcc	hcp	on-top
N	on-top	fcc-like	hcp
C	hcp-like	on-top	fcc
Br	on-top-like	on-top-like	bridge

Rotated

	Threefold 1	Threefold 2	On-top
center	fcc	hcp	on-top
N	on-top-like	fcc-like	hcp-like
C	hcp-like	on-top-like	fcc-like
Br	fcc	hcp	on-top

Summary of computational results

Molecule-substrate interaction energies

$\Delta E = E(\text{TBPT/Au}) - [E(\text{TBPT}) + E(\text{Au})]$

	ΔE / eV		
Model	Threefold 1	Threefold 2	On-top
Non-rotated	-2.97	-2.94	-2.93
Rotated	-3.08	-2.99	-3.17

Stabilization energies were about 3 eV for all cases.
Especially the molecule-substrate interaction becomes strong when Br atoms occupy on-top sites.

Intermolecular interactions

$\Delta E_{\text{molecular}} = E(\text{TBPT, in the same unit cell as TBPT/Au}) - E(\text{TBPT, isolated})$

	$\Delta E_{\text{molecular}}$ / eV	d_{triazine} / Å
Non-rotated	-0.137	15.19
Rotated	-0.054	15.46

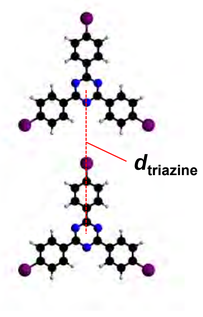

Intermolecular interaction energies calculated using Quantum ESPRESSO are similar magnitude to those by pairwise calculation.

In the case of rotated model, intermolecular distance was extended from molecular pairs without substrate to form stable Br-Au configuration.

→ Br-Au interaction significantly contributes to stability of the phase A.

Conclusion

- We experimentally observed and computationally investigated TBPT/Au(111) adsorption system.
- It is found that one molecular arrangement in which intermolecular Br-N interaction seems dominant (phase A) has high stability (low reactivity to form dimers).
- Therefore in this study we focused on the phase A to understand the origin of the stability.
- DFT calculations revealed the phase A has molecule-substrate interaction energy of 3 eV, while intermolecular stabilization energy is low.
- These results suggests that Br-Au interaction plays an important role to stabilize the phase A, consistent with the experimental findings.

References

[1] Russell, J. C.; *et al. J. Am. Chem. Soc.*, 2011, **133** (12), 4220–4223.
[2] Gatti, R.; *et al. J. Phys. Chem. C* 2014, **118** (44), 25505−25516.
[3] Okada, A.; *et al. in submission.*
[4] Schmidt, M. W.; *et al. J. Comput. Chem.* 1993, **14** (11), 1347–1363.
[5] Giannozzi, P.; *et al. J. Phys.: Condens. Matter.* 2009, **21** (39), 395502.
[6] Giannozzi, P.; *et al. J. Phys.: Condens. Matter.* 2017, **29** (46), 465901.
[7] Grimme, S.; *et al. J. Chem. Phys.* 2010, **132** (15), 154104.
[8] Dal Corso, A. *Comput. Mater. Sci.* 2014, **95**, 337–350.
[9] De Marchi, F.; *et al. Nanoscale* 2019, **11** (41), 19468–19476.